The Analysis of Penumbral Fine Structure
Using an Advanced Inversion Technique

Jan JURČÁK,[1,7] Luis BELLOT RUBIO,[2] Kiyoshi ICHIMOTO,[1] Yukio KATSUKAWA,[1] Bruce LITES,[3] Shin'ichi NAGATA,[4]

Toshifumi SHIMIZU,[5] Yoshinori SUEMATSU,[1] Theodore D. TARBELL,[6] Alan M. TITLE,[6] and Saku TSUNETA[1]

[1]*National Astronomical Observatory of Japan, 2-21-1 Osawa, Mitaka, Tokyo 181-8588*

[2]*Instituto de Astrofísica de Andalucía, Apdo. de Correos 3004, 18080 Granada, Spain*

[3]*High Altitude Observatory, National Center for Atmospheric Research, P.O.Box 3000, Boulder, CO 80307-3000, USA*

[4]*Hida Observatory, Kyoto University, Kamitakara, Takayama, Gifu 506-1314*

[5]*Institute of Space and Astronautical Science, Japan Aerospace Exploration Agency,*

3-1-1 Yoshinodai, Sagamihara, Kanagawa 229-8510

[6]*Lockheed Martin Solar and Astrophysics Laboratory, Bldg. 252, 3251 Hanover St., Palo Alto, CA 94304, USA*

[7]*Astronomical Institute of the Academy of Sciences, Fricova 298, 25165 Ondřejov, Czech Republic*

Abstract

We present a method to study the penumbral fine structure using data obtained by the spectropolarimeter on board Hinode. For the first time, the penumbral filaments can be considered as being resolved in spectropolarimetric measurements. This enables us to use inversion codes with only one-component model atmospheres, and thus to assign the obtained stratifications of the plasma parameters directly to the penumbral fine structure. This approach was applied to the limb-side part of the penumbra in the active region NOAA 10923. Preliminary results show a clear dependence of the plasma parameters on the continuum intensity in the inner penumbra, i.e., a weaker and horizontal magnetic field along with an increased line-of-sight velocity are found in the low layers of the bright filaments. The results in the mid penumbra are ambiguous, and future analyses are necessary to unveil the magnetic field structure and other plasma parameters there.

Key words: methods: data analysis — Sun: sunspots — techniques: polarimetric

1. Introduction

Although the fine structure of penumbra has been studied for a long time, there are only a few confirmed facts regarding the plasma properties and the origin of penumbral filaments. However, the global properties of the magnetic, and velocity structures of the penumbra are well known, i.e., the magnetic field becomes weaker and more horizontal with increasing distance from the sunspot umbra and the velocity field is composed mostly of horizontally oriented Evershed flow, which points outward at photospheric layers (see the review by Solanki 2003, and references therein).

Differences in the plasma parameters of bright and dark filaments were reported for the first time by Beckers and Schröter (1969), who found stronger and more vertical fields in dark filaments. With increasing spatial resolution came other observations that confirmed rapid changes of the inclination and magnetic filed strength on arcsec and sub-arcsec scales (see Solanki 2003, and references therein).

However, the properties of the filamentary structure of the penumbra were derived indirectly from spectropolarimetric measurements (by means of two-component model atmospheres) due to the relatively poor spatial resolution attained by ground-based instruments (see e.g., Bellot Rubio et al. 2004, 2006; Borrero et al. 2004, 2006). Although these analyses found weaker and more horizontal magnetic fields associated with increased velocities, the above properties cannot be ascribed to any specific intensity structures due to a lack of spatial resolution.

Spectroscopic observations at $0\rlap{.}''2$ resolution have revealed some properties of bright penumbral filaments (Bellot Rubio et al. 2005) that are consistent with the indirect analyses described above. Similar results were also obtained by Langhans et al. (2005), who analyzed one-wavelength magnetograms at the same resolution. A direct determination of the vector magnetic field of penumbral filaments could be done for the first time using spectropolarimetric data obtained by Hinode Solar Optical Telescope (SOT).

In this paper, we describe the observations, data reduction, and the inversion method used for a detailed analysis of the penumbral structure. Hopefully, our results will help to distinguish between competitive models of the penumbra (see Bellot Rubio 2007, for a review).

2. Observations

We analysed data obtained using the spectropolarimeter (SP: Tarbell 2007), which is part of the Solar Optical Telescope (SOT: Tsuneta 2007) on board the Hinode satellite (Kosugi 2007).

The instrument observed two iron lines, Fe I 630.15 nm (Landé factor $g = 1.67$) and Fe I 630.25 nm ($g = 2.5$). The diffraction limit of SOT is $0\rlap{.}''3$ at 630 nm. The width of the spectrograph slit is equivalent to $0\rlap{.}''16$, matching the pixel size of the CCD camera. The scanning steps of the spectrograph slit are equivalent to $0\rlap{.}''148$. The wavelength sampling of 2.15 pm
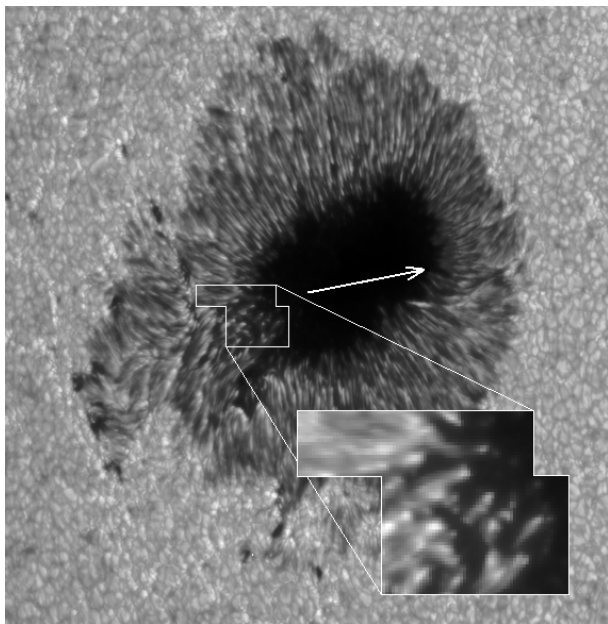
Fig. 1. Map of the continuum intensity reconstructed from the red wing of the Fe I 630.25 nm line. The area under analysis is highlighted and the arrow points to the disc centre.
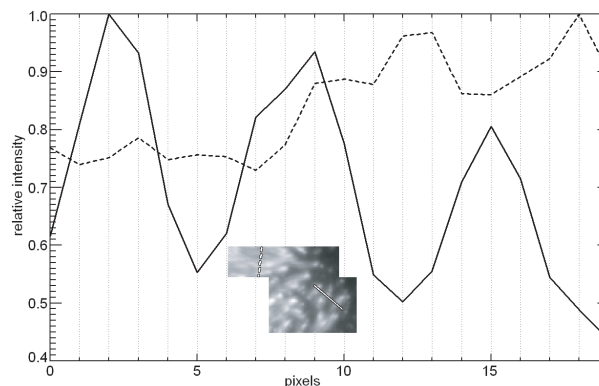

Fig. 2. Two cuts through the filamentary structure of the penumbra, marked in the intensity map in the lower part of the figure. The continuum intensity along these cuts are shown in the plot, where the solid and dashed lines correspond to cuts through the inner and mid penumbra, respectively.

is finer than the spectral resolution of 2.5 pm. The exposure time for one slit position was 4.8 s, during which all Stokes profiles were acquired with a noise level of $10^{-3}I_c$ (where I_c is the continuum intensity). The spatial resolution was slightly worse than the diffraction limit of the telescope due to aliasing induced by the CCD pixel size, but nevertheless reached 0″32.

Dark-field substraction, flat-field division, instrumental polarisation correction, and other data reductions were made using calibration software developed by B. Lites. To prepare the data for the inversion process, a calibration of wavelengths and a normalization of the Stokes profiles to the continuum intensity of the Harvard Smithsonian reference atmosphere (HSRA) had to be performed. We performed this calibration for each slit position separately using the pixels along the slit with a weak polarization signal. The minimum of the Fe I 630.15 nm Stokes I profile averaged over these pixels was used to define the zero velocity, and the continuum intensity of this profile was normalized to HSRA as unity (times the appropriate limb-darkening factor). Following this approach, the photospheric 5-minute oscillations were suppressed to the extent that we did not see any oscillations in the resulting maps of the line-of-sight (LOS) velocity.

On 2006 November 10, the spot in AR 10923 located at heliocentric position 49°E and 6°S was observed. The observed region is shown in figure 1, where the highlighted area, having a size of 14″×10″, was analysed. The arrow points to the disc centre.

In figure 2 we demonstrate that the penumbral filaments were resolved by the SP observations for the first time. There are two cuts through the filamentary structure shown in the lower part of the figure: one in the inner penumbra (solid line) and one in the mid-penumbra (dashed line). We plot the continuum intensity along these cuts. Usually, the brightenings and darkenings occupy at least two pixels (0″32,

i.e., comparable to the spatial resolution of the instrument). Even if the intensity structures are smaller, they still occupy the majority of the resolution element, and thus dominate the line-forming process.

3. Inversion Method

We use a modification of the inversion code SIR (Stokes Inversion based on Response functions), developed at the Instituto de Astrofísica de Canarias (Ruiz Cobo & del Toro Iniesta 1992). This code works under the assumption of local thermodynamical equilibrium and hydrostatic equilibrium. See the survey studies by Ruiz Cobo (1998) or Jurčák (2006).[1] The inversion code synthesises the Stokes profiles coming from an initial model atmosphere, and compares them to the observed ones. Using a least-squares Marquardt's algorithm, the atmospheric model is modified until the difference between the observed and synthetic Stokes profiles (merit function, χ^2) is minimised.

The modification of the SIR code was made by L. Bellot Rubio to allow for any Gaussian perturbation in the stratifications of the plasma parameters along the line of sight, somewhere in the line-forming region. This modified code (Bellot Rubio 2003, hereafter called SIR/GAUSS) uses, by definition, a two-component model atmosphere. The first component represents a background atmosphere with simple stratifications of plasma parameters. The second component is equal to the background atmosphere, but with Gaussian perturbation superposed to it, i.e., the second component can be exactly the same as the first one at some heights, depending on the width and position of the Gaussian.

Figure 3 shows examples of the background temperature stratification (solid black line) and the magnetic field strength stratification (dashed black line) where the Gaussian perturbations are represented by various styles of gray lines. Since we argue that the fine structure of the penumbra is resolved in these SP observations, we set the filling factor of the background component to 0.1% and thus the inversion

---

[1] This can be downloaded at ⟨http://www.asu.cas.cz/~sdsa/jurcak_en.html⟩.
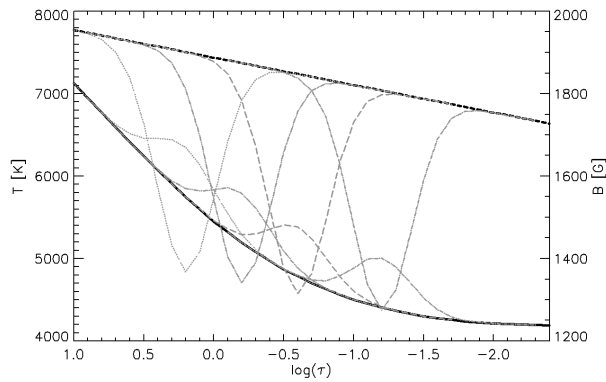
Fig. 3. Background stratifications of the temperature (solid black line) and the magnetic field strength (dashed black line). The various styles of gray lines represent the Gaussian perturbations added to the stratifications of the background model of the atmosphere at four different heights.

code works in practise with a simple one-component model atmosphere.

The original SIR code converged to the same resulting model of the atmosphere almost independently of the initial model. However, the modified code could not change the stratifications of plasma parameters independently as the original one, since there are ties between the parameters induced by the Gaussian perturbation, which must have the same width and position for all of them. Therefore, the resulting model of the atmosphere depends on the starting one, especially on the initial position of the Gaussian perturbation. The Stokes profiles observed in the analyzed region were fitted using four different starting positions for the Gaussian perturbation (see figure 3). The merit functions of the resulting models of the atmosphere were compared at each pixel, and the best solution was used to create maps of plasma parameters.

The starting positions of the Gaussian perturbations were $\log(\tau) = 0.2, -0.2, -0.6$, and -1.2. Except for the height of the Gaussians, the other parameters of the initial guess models were the same: the HWHM, σ, of the Gaussian function was 0.5 in units of the logarithm of the optical depth, the amplitude of the perturbation was $+800$ K for the temperature, -500 G for the magnetic field strength, $+3$ km s^{-1} for the line-of-sight velocity, $-30°$ for the field inclination, and $-5°$ for the field azimuth. The background stratifications were the same in all four cases. In total, the inversion retrieved 13 free parameters.

The initial amplitudes of the Gaussian perturbation were chosen on the basis of two-component inversions of the penumbral fine structure (e.g. Bellot Rubio et al. 2004; Borrero et al. 2006), and because such perturbations can represent currently available theoretical models of the penumbra: the moving flux tube model (Schlichenmaier et al. 1998) and the field-free gap model (Scharmer & Spruit 2006). These two models have similar characteristics from an observational point of view, that is, weaker and rather horizontal fields embedded in a strong and less-inclined background field. The moving flux tube model predicts that the weak fields are associated with increased velocities. Gaussian perturbations with initial amplitudes, such as the ones used here, can simulate the top of field-free gaps or low-lying penumbral flux tubes if they are

positioned around the continuum-forming layer [$\log(\tau) = 0.2$ or -0.2], or penumbral flux tubes if they are located higher in the line-forming region.

4. Penumbral Fine Structure

Since only a small part of the penumbra was analyzed and the studied area did not cover the whole width of the penumbra, no general conclusions about the penumbral structure are made here. We selected this region because many clearly defined bright filaments enter the umbra, enabling us to study their plasma properties with high precision using the method described above. Moreover, the Stokes V profiles observed in the limb-side penumbra at a given position on the solar disc are highly asymmetric. The asymmetries can be explained only with gradients of velocity and magnetic field in the line-forming region, and thus the presence of Gaussian perturbations in the stratifications of these plasma parameters is necessary because the gradients in the background component are too small to produce such asymmetric profiles.

Figure 4 shows two examples of the observed profiles. The upper row displays Stokes I and V profiles observed in the inner penumbra (solid lines) together with the synthetic profiles and stratifications of the magnetic field strength, inclination, and LOS velocity obtained using the SIR/GAUSS code with the starting position of the Gaussian perturbation at $\log(\tau) = 0.2$ (dotted lines) and $\log(\tau) = -1.2$ (dashed lines). The same applies to the lower row, where a pixel from the mid penumbra was studied.

The inclination was evaluated with respect to the line of sight in these plots. We could see that the inclination of the background field is in both cases close to $90°$, and thus the V profiles generated by this component are weak. In the inner penumbra the background component has an opposite polarity with respect to the Gaussian component (it is slightly larger than $90°$) and that together with the velocity difference are the main reasons for the asymmetric V profile. Because the polarity of the background and Gaussian components are the same in the mid-penumbra, we do not see any V lobe cancellation, and the asymmetry is caused only by the difference in the LOS velocities.

The solution in the inner penumbra is easy to interpret, because the best fits are always obtained using Gaussian perturbations deep in the atmosphere. In the example shown in the upper row of figure 4, the merit function is 12.3 for the solution obtained with a Gaussian perturbation low in the atmosphere, compared to $\chi^2 = 22.6$ for that obtained with a Gaussian located higher in the line-forming region.

On the other hand, the correct solution in the mid penumbra is much harder to find. In the example of figure 4, the fit obtained using the initial perturbation high in the atmosphere is better [$\chi^2 = 18.2$ for $\log(\tau) = -1.2$ vs. $\chi^2 = 25.9$ for $\log(\tau) = 0.2$], although the shown fits to the Stokes I and V profiles appear to have a similar quality. Generally, the variations in merit functions obtained with different starting heights for the Gaussian perturbations are not significantly different in the mid-penumbra, and thus it is difficult to decide which solution is closer to reality. Moreover, the fits are generally worse in the mid-penumbra,
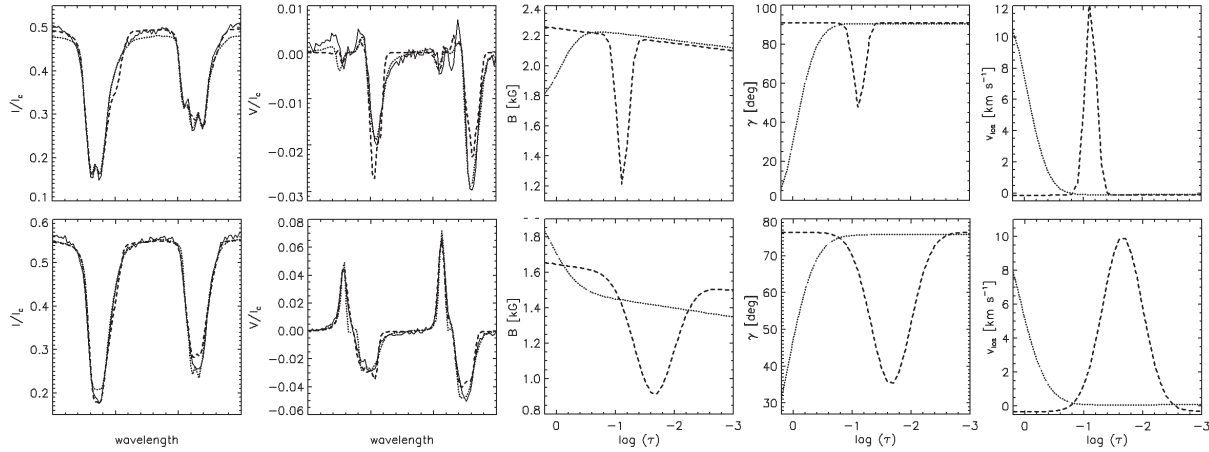
Fig. 4. Observed Stokes I and V profiles (solid lines) plotted together with the synthetic profiles and stratifications of the magnetic field strength, inclination, and LOS velocity obtained using the SIR/GAUSS code with the starting position of the Gaussian perturbation at $\log(\tau) = 0.2$ (dotted lines) and $\log(\tau) = -1.2$ (dashed lines). The upper row shows an example of the profiles observed in the inner penumbra, where the mid-penumbra is represented by the profiles displayed in the lower row.
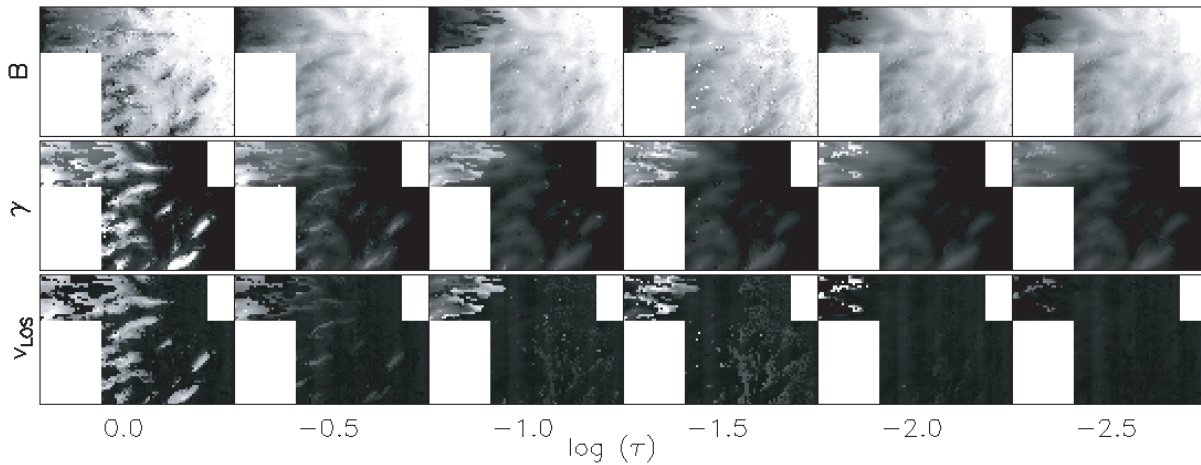

Fig. 5. Resulting maps of the magnetic field strength, inclination, and LOS velocity (from top to bottom) at different heights in the atmosphere. The colour codes for the displayed plasma parameters are the same as in figure 6 (see the colour bars there).

where the mean value of the merit function is 33, than in the inner penumbra, where the mean value of χ^2 is 19.

In figure 5 we show the resulting maps of the magnetic field strength (upper row), inclination (middle row), and LOS velocity (lower row) at six optical depths. These maps were created from the best solutions, which were obtained at each point (selected on the basis of the merit function).

This figure clearly shows discontinuities in the values of the plasma parameters in the mid-penumbra (upper-left part of the analyzed region). The problem is that solutions with a Gaussian perturbation located low and high in the line-forming region reproduce the observed Stokes profiles with similar quality, and do have different stratifications of the plasma parameters (although the resulting stratifications of the background component are similar). At some areas in the mid-penumbra we found a weaker, more horizontal magnetic field together with increased LOS velocities high in the atmosphere [around $\log(\tau) = -1.5$]. A typical example of such a solution is the pixel presented in the lower part of figure 4 (dashed line).

At other areas the best fit corresponds to the location of the Gaussian perturbation low in the atmosphere, i.e., the field is more horizontal and the LOS velocities are increased there. However, for this type of solution the magnetic field strength is either slightly larger, or remains basically the same as in the background component (i.e., the amplitude of the Gaussian perturbation in field strength is small, see the dotted line in the lower part of figure 4 as an example).

As can be seen, the solution is clear in the inner penumbra, where the best fits correspond to the Gaussian perturbation low in the atmosphere. The bright filaments protruding into the umbra have lower magnetic field strengths, more horizontal fields, and significantly larger LOS velocities. Similar conclusions can be made on the basis of figure 6, where the stratifications of various plasma parameters are shown along a cut that crosses four bright structures in the inner penumbra (see the caption of this figure for details). In figures 5 and 6, the inclination has been transformed to the local reference frame, i.e., it is measured from the local normal
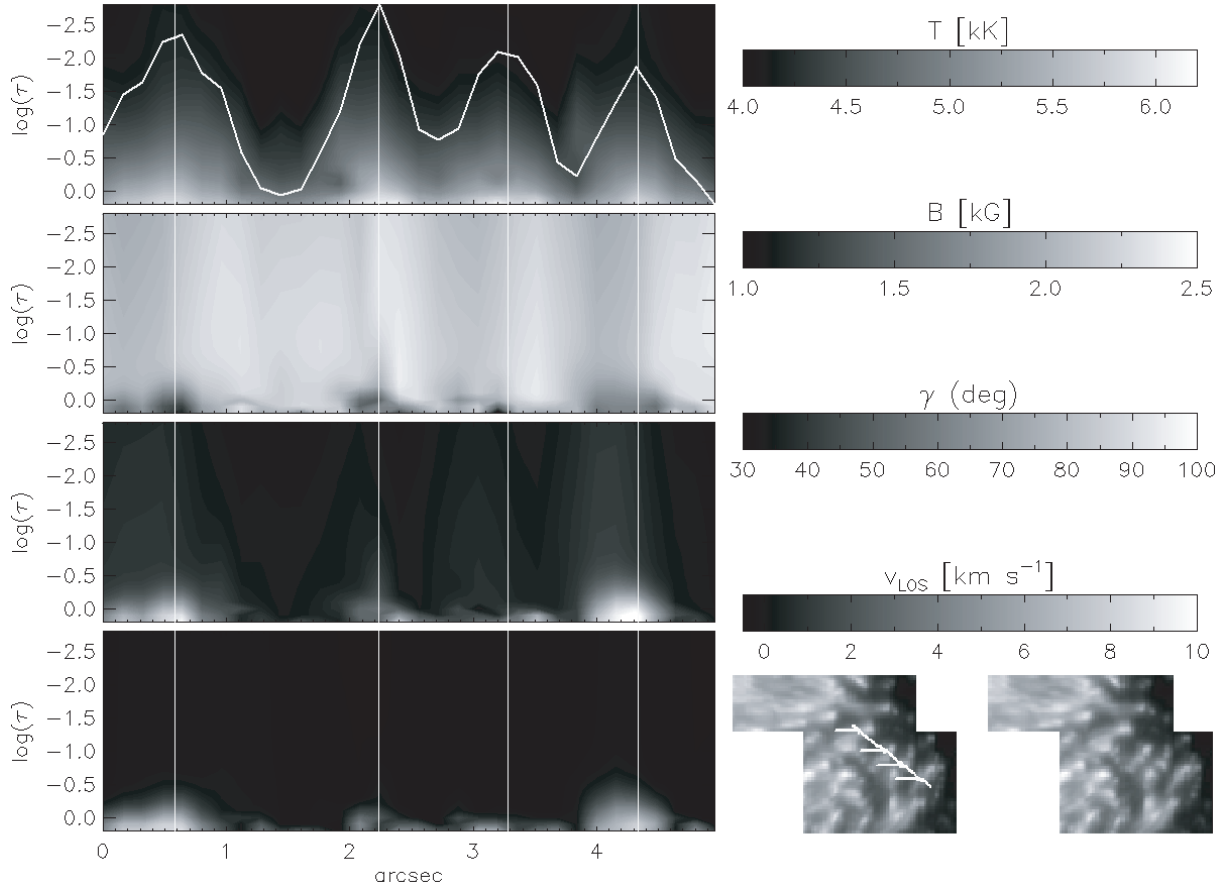
Fig. 6. Vertical cut through four bright structures in the inner penumbra. The position of the cut is indicated in the continuum intensity map in the lower-right part of the figure. The left part of the figure shows the stratifications of the temperature, magnetic field strength, inclination, and LOS velocity (from top to bottom) along this cut, where the right part of the figure displays the colour bars of these plasma parameters. The white line in the temperature stratification map corresponds to the continuum intensity along the cut. The vertical lines in the maps of stratifications correspond to the arrows in the continuum intensity map.

line pointing downwards.

In the case of the magnetic field inclination and LOS velocities, the background stratifications are not significantly influenced by the presence of bright structures, and reach similar values as in the surrounding umbra, i.e., the filamentary structure almost disappears higher in the atmosphere. In the case of stratifications of the magnetic field strength, the filamentary structure is sharpest low in the atmosphere, but do not disappear with height. This could be an artifact of the inversion technique, but it remains to be tested.

In the upper map of figure 6 we show the temperature along the cut; the white line represents the continuum intensity along the cut. We can clearly see that the bright structures have naturally higher temperatures low in the atmosphere. The increase of the temperature in such structures is imperative, but the absolute values of the temperature enhancement cannot always be trusted, because we occasionally do not fit the continuum of the Stokes I profile correctly (mostly because the macro-turbulence, the helping parameter for the line broadening, is set to zero, and thus an increase of the temperature at lower layers would result in a better fit of the continuum intensity, but a worse fit of the line wings).

Here, we make the first rough estimates of the difference between the values of the plasma parameters in the bright filaments and the surrounding umbra. The parameters given below correspond to an optical depth of $\log(\tau) = -0.2$, where the results of the inversion are more reliable than at the optical depth unity layer, itself. The uncertainties in the plasma parameters are not discussed here, but are much smaller than the differences that we found.

The estimates were made from the bright filaments, whose cut is analyzed in figure 6. In the case of the magnetic field strength, we found a decrease of approximately 600 G (1700 G in the bright filaments compared to 2300 G in the surrounding umbra). This value is similar to those deduced from two-component inversions performed by Bellot Rubio et al. (2004) and Borrero et al. (2006), i.e., 500 G and 1500 G respectively. In the inner penumbra, these authors found magnetic field inclinations of around 20° and 60° in the background and the flux-tube components, respectively. The values in the surrounding umbra should be comparable to those of the background atmosphere in two-component inversions, and indeed we find values of around 30°. However, the field inclinations in bright filaments are around 90° in our case, larger than those derived from two-component inversions. As expected, the LOS velocities are close to zero in the umbra

surrounding the bright filaments, and reach values of around 4 km s^{-1} in them. These large velocities are again compatible with the results of Bellot Rubio et al. (2004) and Borrero et al. (2006), who found values of 5 and 3 km s^{-1} in the flux-tube component for spots at similar heliocentric angles (40°, resp 37°). The most important point is that we can directly ascribe these properties to the bright penumbral filaments. That was not possible with the results of the two-component inversions mentioned above.

5. Conclusions

We introduced a method to analyse the data obtained by SP on board Hinode using an advanced inversion technique. We applied this method to the limb-side penumbra of Active Region 10923, observed on 2006 November 10. This allowed us to directly obtain the structure of the magnetic field vector together with the velocity configuration of the penumbral fine structure. This was possible for the first time, and our preliminary results for the inner penumbra confirm previous results coming from two-component inversions of visible and near-infrared lines. However, inversion techniques have so far been unable to relate the magnetic structures represented by the two components with intensity structures. This had to be done with the help of spectroscopic data or magnetograms, which have better spatial resolution.

Using SP data from Hinode SOT, we found that the magnetic field in the bright filaments is weaker by some 600 G compared with the surrounding umbra at an optical depth of $\log(\tau) = -0.2$. The field is horizontal in those layers and the LOS velocity reaches values of around 4 km s^{-1}. The differences between the plasma parameters in the bright filaments and the surrounding umbra quickly decrease with the height and disappear around $\log(\tau) = -0.5$. This means that the bright filaments are structures located deep in the atmosphere in the inner penumbra, and that the background magnetic field closes above them. To some extent, such a result is similar to that found in light bridges (Jurčák et al. 2006).

This could support the theory of a field-free gappy penumbra (Scharmer & Spruit 2006) which hypothesises that bright penumbral filaments and light bridges are representations of the same phenomena (top of field-free gaps) of different magnitude. However, our results could also be explained by flux tubes located around optical depth unity in the inner penumbra, as predicted by the moving-tube model of Schlichenmaier et al. (1998).

The advantage of this model is that strong Evershed flows channeled by the tubes arise naturally from the calculations, whereas the gappy model does not offer any explanation for the Evershed flow. One of the arguments against the moving-tube model is a large predicted outflow velocity of around 13 km s^{-1}; here, we have found similar magnitudes of velocities in the mid-penumbra. For example 11 km s^{-1}, if we compute the outflow velocity as $v_{\mathrm{LOS}}/\cos(\gamma_{\mathrm{LOS}})$, and take the value of the LOS velocity to be 7 km s^{-1} and the LOS inclination to be 50° (selected on the basis of the pixel from mid penumbra shown in figure 4, dashed lines, where we do not use the peak values, because they are probably overestimated). See Ichimoto et al. (2007) for other arguments supporting the moving flux tube model on the basis of Hinode observations.

The results in the mid-penumbra are more difficult to interpret. There are two possible solutions that fit the observed Stokes profiles with similar quality. According to the rising flux tube model, the tubes should be positioned higher in the atmosphere in the outer penumbra, and thus a more careful and detailed analysis of this region is needed to test the realism of the two most-discussed models of the penumbral fine structure.

References

Beckers, J. M., & Schröter, E. H. 1969, Sol. Phys., 10, 384
Bellot Rubio, L. R. 2003, in ASP Conf. Ser., 307, ed. J. Trujillo-Bueno & J. Sanchez Almeida (SanFransisco: ASP), 301
Bellot Rubio, L. R. 2007, in Highlights of Spanish Astrophysics IV, ed. F. Figueras, J. M. Girart, M. Hernanz, & C. Jordi (Dordrecht: Springer), 271
Bellot Rubio, L. R., Balthasar, H., & Collados, M. 2004, A&A, 427, 319
Bellot Rubio, L. R., Langhans, K., & Schlichenmaier, R. 2005, A&A, 443, L7
Bellot Rubio, L. R., Schlichenmaier, R., & Tritschler, A. 2006, A&A, 453, 1117
Borrero, J. M., Solanki, S. K., Bellot Rubio, L. R., Lagg, A., & Mathew, S. K. 2004, A&A, 422, 1093
Borrero, J. M., Solanki, S. K., Lagg, A., Socas-Navarro, H., & Lites, B. 2006, A&A, 450, 383

Ichimoto, K., et al. 2007, PASJ, 59, S593
Jurčák, J. 2006, Doctoral Thesis, Charles University, Prague
Jurčák, J., Martínez Pillet, V., & Sobotka, M. 2006, A&A, 453, 1079
Kosugi, T., et al. 2007, Sol. Phys., 243, 3
Langhans, K., Scharmer, G. B., Kiselman, D., Löfdahl, M. G., & Berger, T. E. 2005, A&A, 436, 1087
Ruiz Cobo, B. 1998, Ap&SS, 263, 331
Ruiz Cobo, B., & del Toro Iniesta, J. C. 1992, ApJ, 398, 375
Scharmer, G. B., & Spruit, H. C. 2006, A&A, 460, 605
Schlichenmaier, R., Jahn, K., & Schmidt, H. U. 1998, A&A, 337, 897
Solanki, S. K. 2003, A&AR, 11, 153
Tarbell, T., et al. 2007, Sol. Phys.   submitted
Tsuneta, S., et al. 2007, Sol. Phys.   submitted